Applied Catalysis B: Environmental 117–118 (2012) 275–282

Contents lists available at SciVerse ScienceDirect

Applied Catalysis B: Environmental

journal homepage: www.elsevier.com/locate/apcatb

NO_x reduction by H_2 on WO_x/ZrO_2-supported Pd catalysts under lean conditions

Melanie Leicht[a], Florian J.P. Schott[a], Michael Bruns[b], Sven Kureti[c,*]

[a] Karlsruhe Institute of Technology, Institute of Technical Chemistry and Polymer Chemistry, D-76128 Karlsruhe, Germany
[b] Karlsruhe Institute of Technology, Institute for Applied Materials, D-76344 Eggenstein-Leopoldshafen, Germany
[c] Technical University Bergakademie Freiberg, Department of Energy Process Engineering and Chemical Engineering, Fuchsmühlenweg 9, D-09596 Freiberg, Germany

ARTICLE INFO

Article history:
Received 8 October 2011
Received in revised form 17 January 2012
Accepted 18 January 2012
Available online 28 January 2012

Keywords:
NO_x reduction by H_2
Catalyst
Pd
WO_x
ZrO_2

ABSTRACT

This work addresses the H_2-deNO_x reaction representing a prospective tool for the low-temperature NO_x abatement under lean conditions. A novel $Pd/WO_x/ZrO_2$ catalyst with a W content of 8.7% was developed. The screening of the Pd load performed by temperature-programmed reaction on a laboratory bench provided highest efficiency at a Pd content of 0.41% (0.41Pd/W/ZrO_2). This catalyst showed considerable H_2-deNO_x activity between 125 and 280 °C with an outstanding overall N_2 selectivity of 96%. Drastically higher performance was observed when 0.41Pd/W/ZrO_2 was evaluated under steady-state conditions resulting in 90% deNO_x at 160 °C and a space velocity of 80,000 h^{-1}. At this temperature, the apparent turnover frequency of Pd amounted to 8.1×10^{-5} s^{-1}, which was very close to that of Pt existing in the highly active Pt/W/ZrO_2 system. The variation of the H_2 and O_2 feed concentration indicated that growing H_2 led to increasing H_2-deNO_x performance accompanied by decreasing N_2 selectivity. O_2 did not affect the selectivity, but clearly limited the operation window of the catalyst at O_2 contents above 6 vol.%. The presence of H_2O as well as hydrothermal exposure at 750 °C declined both activity as well as N_2 selectivity.

The characterisation of the 0.41Pd/W/ZrO_2 catalyst by XRD, HRTEM/EDX and XPS showed tetragonal ZrO_2, whilst tungsten likely exists in sub-monolayer WO_x entities as well as amorphous WO_3 nanoparticles. Pd was predominately present in the form of PdO with particle sizes below 2 nm.

Mechanistic studies conducted by DRIFT spectroscopy indicated that the lean H_2-deNO_x reaction 0.41Pd/W/ZrO_2 occurs on the Pd sites. The reaction is considered to follow the mechanism according to Burch implying pre-reduction of the active sites by H_2 followed by NO dissociation and formation of N_2 with minor production of N_2O. However, some participation of NO_x species located on the W/ZrO_2 substrate cannot be ruled out completely.

© 2012 Elsevier B.V. All rights reserved.

1. Introduction

The most important anthropogenic origin of pollutants is the combustion of fossil energy sources like coal, natural gas, oil and fuel. In the combustion process, carbon dioxide (CO_2) and water (H_2O) form as the major products, but to some extent pollutants such as carbon monoxide (CO), nitrogen oxides (NO_x) and hydrocarbons (HC) are produced as well. The preferred way to minimise these air pollutants is the optimisation of the combustion. Despite this, the emission control by catalytic techniques is more and more required to meet current and future legislation limits.

The most frequent application of exhaust catalysis is the so-called three way catalyst (TWC) used in gasoline engines since the 1980s. TWC systems contain Pt/Rh or Pd/Rh as active components simultaneously converting NO_x, CO, H_2 and HC into N_2, CO_2 and H_2O. The TWC process exclusively occurs within a narrow range of O_2 content being close to stoichiometric combustion conditions [1,2]. The transfer of the TWC technology to lean burn engines, i.e. lean gasoline and diesel motors, is problematic, because of its insufficient potential for the abatement of NO_x. This feature is associated with the lower raw emissions of reducing agents as well as the excess of O_2, which enhances the oxidation of HC and CO thus suppressing deNO_x. Therefore, alternative concepts are required for the reduction of NO_x under oxygen-rich conditions being relevant for stationary industrial processes as well. For lean NO_x removal in automobiles, the selective catalytic reduction by NH_3 (SCR) and NO_x storage reduction catalysts (NSR) are actually considered [1,2]. SCR is the classical NO_x abatement technology employed since the early 1970s in power plants. The most common SCR catalyst used today is TiO_2-supported WO_3/V_2O_5 [3]. Moreover, for automobiles Fe and Cu based zeolite catalysts are currently taken into consideration [4,5]. These catalysts drastically enhance the deNO_x reaction in the presence of NO_2 providing high performance below ca. 230 °C [6].

* Corresponding author. Tel.: +49 3731 39 4482; fax: +49 3731 39 4555.
E-mail address: kureti@iec.tu-freiberg.de (S. Kureti).

0926-3373/$ – see front matter © 2012 Elsevier B.V. All rights reserved.
doi:10.1016/j.apcatb.2012.01.023

NSR catalysts were originally developed for lean spark-ignition engines and are actually applied for diesel passenger cars. The NSR procedure is based upon the periodic adsorption and reduction of NO_x [7]. The catalysts consist of precious metals, i.e. Pt, Pd and Rh, and basic adsorbents like Al_2O_3, CeO_2 and $BaCO_3$ [8]. In the lean phase of the engine, NO_2 is stored by the basic components of the NSR. When its storage capacity is reached, rich exhaust conditions are established momentarily by engine management systems. Hereby, NO_x desorbs from the substrate and is reduced on the precious metals by the reducing agents being present in excess then. A unique after-treatment technique is the Bluetec I system from Daimler, which includes a NSR and a downstream SCR catalyst fed by NH_3 produced on the NSR catalyst upon the rich phase.

A constraint of automotive SCR and NSR is the rather limited efficiency at low temperatures, i.e. below approximately 170 °C. This is associated with the kinetic inhibition of the Pt-catalysed formation of the key molecule NO_2. Contrary, the catalytic reduction of NO_x by H_2 (H_2-deNO_x) offers a high potential for the low-temperature regime. Possible applications of lean H_2-deNO_x are diesel passenger cars, fossil power plants, waste combustion plants, nitric acid production and air separation systems. Since the 1970s a series of Pt H_2-deNO_x catalysts was presented exhibiting considerable activity below 170 °C even under strongly oxidising conditions [9–13]. A serious constraint is their narrow operation window and the significant formation of N_2O. However, in recent years, Costa et al. [14–17] reported on Pt/$La_{0.7}Sr_{0.2}Ce_{0.1}FeO_3$ and Pt/MgO-CeO_2 catalysts with pronounced low-temperature activity as well as substantially advanced N_2 selectivity up to 80–90%. Moreover, we presented a Pt/WO_x/ZrO_2 catalyst revealing marked H_2-deNO_x performance between 50 and 450 °C and high N_2 selectivity up to 90% [18]. In addition to the above-mentioned classical heterogeneous catalysts, electrochemically supported Pt and Pt/Rh catalysts were also suggested for lean H_2-deNO_x using a proton conducting substrate [19].

Also, a couple of Pd H_2-deNO_x catalysts were lately referred, partially with remarkable N_2 selectivity, but limited performance as compared to the best Pt samples [12,20–22]. The most active Pd systems are Pd/$LaCoO_3$ prepared by flame-spray pyrolysis [22,23] and Pd supported by pillared interlayered clays [21]. Furthermore, it should be mentioned that pre-reduced Pd is known to decompose NO under lean conditions [24].

The major focus of this work lay in the advancement of the N_2 selectivity of the catalytic H_2-deNO_x reaction under oxygen-rich conditions. For this purpose, a series of Pd/WO_x/ZrO_2 catalysts was systematically prepared and studied. This catalytic material was taken to combine the WO_3/ZrO_2 substrate recently engineered for highly active Pt catalysts [18] with the precious metal component Pd potentially enhancing the N_2 formation [19–21]. This approach involved the variation of the Pd content of the catalysts implying kinetic tests as well as physical–chemical characterisation. As reference materials, classical Pt/Al_2O_3 and Pd/Al_2O_3 samples as well as Pt/WO_x/ZrO_2 were taken. Furthermore, the most effective catalyst was evaluated towards its practical potential and some mechanistic studies were made to provide insights into the course of the lean H_2-deNO_x reaction.

2. Experimental

2.1. Preparation and characterisation of the catalysts

The Pd/WO_x/ZrO_2 catalysts were prepared with a W load of 8.7%, whilst the Pd content was varied from 0.14, 0.27, 0.41, 0.55, 0.68 to 0.82% (Pd and W loads refer to bare ZrO_2). The W loading was adopted from the relating Pt/WO_x/ZrO_2 system [18]. The ZrO_2 carrier was modified by tungsten oxide and palladium by using the incipient wetness method as described in detail recently [18]. Briefly, tetragonal ZrO_2 (S_{BET} = 70 m^2 g^{-1}) synthesised by an advanced hydrazine route was impregnated with a defined volume of a $(NH_4)_6H_2W_{12}O_{41}$ solution (Fluka), such that it was completely absorbed. After overnight drying at 100 °C, the sample was modified by Pd as done for tungsten oxide using a solution of $Pd(NO_3)_2$ (Chempur). Subsequently, the sample (7 g) was dried overnight at 100 °C and activated for 30 min at 300 °C by dosing a mixture of 14 vol.% H_2 and 86 vol.% N_2 at a flow rate of 500 ml min^{-1}. Finally, the catalyst was conditioned in static air atmosphere at 500 °C for 5 h. The Pd/Al_2O_3, Pt/Al_2O_3 and Pt/WO_x/ZrO_2 reference catalysts were prepared in similar way exhibiting a load of 0.41% Pd and 0.25% Pt, respectively (1922 μmol Pd and 640 μmol Pt per 500 mg catalyst) and 11% W; the γ-Al_2O_3 support was a commercial product from Sasol with a BET surface area of 165 m^2 g^{-1}.

The sample codes used throughout this paper refer to the content of precious metal as well as the type of substrate, e.g. 0.14Pd/W/ZrO_2 for the ZrO_2 based sample with a load of 0.14% Pd and 8.7% W.

The catalysts were characterised by N_2 physisorption (BET), powder X-ray diffraction (PXRD), high-resolution transmission electron micrography (HRTEM) and X-ray photoelectron spectroscopy (XPS). The BET surface area of the catalysts was investigated by multi-point BELSORP-mini II using N_2 as adsorbate. The sample was pre-treated at 300 °C for 2 h in vacuum (10^{-4} mbar) and cooled to −196 °C, and then the N_2 isotherm was recorded. From the adsorption data recorded at p/p_0 ratios between 0.05 and 0.30 the BET surface area (S_{BET}) was derived. PXRD patterns were recorded at room temperature on a Siemens 501 using Ni filtered Cu Kα radiation. A 2Θ step size of 0.02 was used with an integration time of 4 s. Bright field HRTEM images were taken with a Philipps CM200 FEQ equipped with an EDX detector. For the analysis, a dispersion with iso-propanol was prepared being dropped on a grid coated by silicium. After drying at ambient conditions, the HRTEM analysis was started.

XPS measurements were performed using a K-Alpha XPS spectrometer from ThermoFisher Scientific. Data acquisition and processing using the Thermo Avantage software is described elsewhere [25]. All samples were analysed using a microfocused monochromated Al Kα X-ray source (30–400 μm spot size). The K-Alpha charge compensation system was employed during analysis using electrons of 8 eV energy and low-energy argon ions to prevent any local charging. The spectra were fitted with one or more Voigt profiles (BE uncertainty: ±0.2 eV). The analyser transmission function, Scofield sensitivity factors and effective attenuation lengths (EALs) for photoelectrons were applied for quantification [26]. EALs were calculated using the standard TPP-2 M formalism [27]. All spectra were referenced to the C 1s peak of adventitious carbon at 285.0 eV binding energy controlled by means of the well-known photoelectron peaks of metallic Cu, Ag, and Au, respectively.

2.2. H_2-deNO_x studies

For the kinetic H_2-deNO_x tests, respective catalyst was pressed to pellet with 40 MPa, granulated and sieved to a size of 125 to 250 mm. This was done to avoid discharge of sample mass upon the catalytic runs. The measurements were performed on a laboratory bench using a quartz glass tube reactor (i.d. 8 mm) and adjusting a total flow (F) of 500 ml min^{-1} (STP). The stainless steel pipes of the bench were kept at 150 °C to avoid condensation of water. A sample mass (m_{cat}) of 500 mg was taken resulting in a space velocity (S.V.) of 80,000 h^{-1}. The catalyst was used in form of a packed bed fixed by quartz wool. Before the studies, the sample was pre-treated in Ar flow at 500 °C for 15 min to remove possible contaminants, e.g. CO_2 and hydrocarbons, thus establishing reproducible reaction conditions.

The catalysts were evaluated by temperature-programmed reaction; after the pre-treatment, the feed was added and temperature was decreased to ca. 50 °C with a rate (β) of 2 K min^{-1}. This rather slow rate excluded measurable NO_x storage effects; only below 80 °C slight interference of NO_x adsorption on the substrate was found corresponding to less than 10% conversion. The standard feed consisted of 500 vppm NO_x (480 vppm NO, 20 vppm NO_2), 2000 vppm H_2, 6 vol.% O_2 and Ar as balance. The feed was obtained by blending special mixtures of 9000 vppm H_2 in Ar and 3000 vppm NO in Ar with pure O_2 and Ar (Air Liquid) using mass flow controllers (MKS Instruments). Moreover, for examination of the potential of the most effective catalyst the concentration of H_2 and O_2 was systematically varied and H_2O was added to the feed. Water vapour was produced in a parallel line of the dosing system by oxidation of H_2 on a Pt/Al_2O_3 catalyst. This co-flow was blended with the main flow before the reactor section. For the evaluation of the hydrothermal stability, the most prospective catalyst (500 mg, fixed bed) was exposed for 24 h at 750 °C to a feed (500 ml min^{-1}, STP) comprised of 10 vol.% H_2O and 10 vol.% O_2 with N_2 as balance. These conditions refer to a typical worst case aging scenario for diesel passenger car applications.

The gas inlet and outlet temperature of the reactor was measured by two K-type thermocouples, each centred directly in front of and behind the catalyst bed. The temperature difference between inlet and outlet was always below 10 K. The gas-phase analysis of NO_x was conducted by chemiluminescence (EL-ht, EcoPhysics), whilst N_2O was detected by non-dispersive infrared spectroscopy (Uras 10E, Hartmann & Braun). Oxygen was checked by using magnetomechanics (Magnos 6 G, Hartmann & Braun). In special studies, NO_x, N_2O, NH_3 and H_2O were monitored by hot measuring Fourier transform infrared spectroscopy (Multigas Analyzer 2030, MKS Instruments). In addition to the temperature programmed runs, some investigations were performed under steady-state conditions. In these stationary experiments, a GC/TCD analyser (RGC 202 with packed columns Haye Sep Q 60 and mol sieve 5 Å, Siemens) was used for the detection of N_2 taking Ar as balance gas.

It was estimated that neither pore diffusion (Weisz Prater criterion < 10^{-2} [28]) nor film diffusion (Mears criterion < 10^{-5} [29]) affected the H_2-deNO_x kinetics under the reaction conditions established. The Weisz Prater criterion expresses the ratio of the effective rate of reaction and pore diffusion, whilst the Mears criterion demonstrates the ratio of the effective rate of reaction and film diffusion; both criteria refer to respective gas-phase concentration and catalyst particle size.

The catalytic activity is expressed in terms of NO_x conversion ($X(NO_x)$), which refers to the formation of N_2 and N_2O, i.e. $X(NO_x) = (2c(N_2) + 2c(N_2O))/c(NO_x)_{in}$. The mass of N is always balanced by the production of N_2 and N_2O excluding the genesis of NH_3. Therefore, in the temperature programmed studies the concentration of N_2 is derived from the NO_x and N_2O traces, i.e. $c(N_2 = (c(NO_x)_{out} - 2c(N_2O))/2$. This approach was checked by preliminary H_2-deNO_x investigations using GC/TCD for N_2 analysis. As mentioned above, only below 80 °C a negligible difference between measured and calculated N_2 concentration was obtained due to NO_x storage effects. The selectivity of N_2 ($S(N_2)$) is defined as $S(N_2) = c(N_2)/(cN_2) + c(N_2O))$ corresponding expression is used for N_2O ($S(N_2O)$). For the direct comparison of different catalysts, the overall NO_x conversion ($S(N_2)_{ov}$) and overall N_2 selectivity ($S(N_2)_{ov}$) is also given: and $S(N_2)_{ov} = \int_{T_1}^{T_2} S(N_2)dT/(T_2 - T_1)$ and $S(N_2)_{ov} = \int_{T_1}^{T_2} S(N_2)dT/(T_2 - T_1)$. T_1 and T_2 delimit the range of NO_x conversion exceeding 20% thus minimising error propagation. Furthermore, the maximum NO_x conversion ($X(NO_x)_{max}$), temperature of maximum deNO_x (T_{max}) and operation window expressed as temperature range with NO_x conversions above 20% ($T_{x>20}$) are taken for reference purposes. For the comparison of the specific activity of Pd and Pt, the apparent turnover frequency (TOF) is used. Apparent TOF is defined as the molar amount of NO_x being converted per total number of precious metal atoms and time.

2.3. DRIFTS studies

The diffuse reflectance infrared Fourier infrared spectroscopic (DRIFTS) studies were performed on a Nicolet 5020 FTIR spectrometer (Thermo) equipped with a MCT detector and DRIFTS optics (P/N 19930, Specac). The IR cell contained a ZnSe window and was adapted to a gas-dosing system being similar to that described in the previous section. The spectra were recorded in the range from 1000 to 4000 cm^{-1} with an instrument resolution of 4 cm^{-1}. The catalyst was used in powder form.

In the DRIFTS studies, the H_2-deNO_x reaction was sequentially examined. Firstly, the catalyst was charged into the sample holder of the cell and was pre-treated at 500 °C in N_2 flow (500 ml min^{-1}, STP) as done in the catalytic studies (Section 2.2). Then, it was cooled to the reaction temperature under flowing N_2 and the background spectrum was acquired. Subsequently, the sample was exposed to a flow of 500 vppm NO_x (480 vppm NO, 20 vppm NO_2) and 6 vol.% O_2 (N_2 balance) until saturation was reached followed by purging with N_2 for 10 min. After this, a blend of 500 vppm H_2 and 6 vol.% O_2 in N_2 was added. The H_2 concentration was reduced to 500 vppm to avoid hot spots on the catalyst. Spectra were continuously collected whilst accumulating 100 scans. This resulted in a time resolution of ca. 2 min.

The DRIFT spectra are presented in terms of Kubelka–Munk transformation being defined as $F(R) = (1 - R)^2/(2R)$ with $R = R_s/R_b$. R_s is the reflectance of the reacted sample and R_b that of the background.

3. Results and discussion

3.1. Characterisation and H_2-deNO_x performance of the catalysts

Preliminary H_2-deNO_x investigations performed without catalyst provide no deNO_x excluding any blind effects. Contrary, the $0.25Pt/Al_2O_3$ reference catalyst reveals pronounced low-temperature activity, whereas its operation window is rather narrow ranging from 50 to 150 °C. Moreover, N_2O forms as the major product; $S(N_2)_{ov}$ amounts to 20% only (Fig. 1, top). The lean H_2-deNO_x performance of $0.25Pt/Al_2O_3$ is in fair agreement with results reported in the literature [9,10]. As expected, the benchmark of $0.25Pt/W/ZrO_2$ reveals markedly improved catalytic efficiency implying a broader operation window ($T_{x>20}$ = 65–325 °C), higher maximum NO_x conversion ($X(NO_x)_{max}$ = 90%) and higher overall N_2 selectivity ($S(N_2)_{ov}$ = 70%) (Fig. 1, bottom). In contrast to that, the $0.41Pd/Al_2O_3$ reference, which exhibits three times more precious metal (1922 μmol) compared to the two Pt references, shows very minor H_2-deNO_x activity. Its NO_x conversion is below 15% in the entire temperature regime.

Table 1 demonstrates the most important H_2-deNO_x features of all the $Pd/W/ZrO_2$ catalysts along with their total amount of Pd and BET surface area. The X-ray diffractograms of these samples exclusively evidence tetragonal ZrO_2, whereas no reflexes appear, which might be ascribable to palladium, palladium oxide or tungsten oxide. In the XPS analyses, the catalysts reveal an absorption signal at 36.2 eV corresponding to the $W4f_{7/2}$ transition of W^{6+} species. Furthermore, the HRTEM images exemplarily taken for $0.41Pd/W/ZrO_2$ show neither crystalline entities nor agglomerates of tungsten oxide, whilst EDX indicates tungsten all over the sample. These findings of XRD and HRTEM/EDX are in line with literature dealing with WO_x/ZrO_2. According to Wachs the present load of W refers to a surface concentration of about

Table 1
Molar amount of Pd[a], BET surface area and H_2-deNO$_x$ features[b] of the Pd/WO_3/ZrO_2 catalysts; the W load is 8.7%.[c]

Catalyst	n(Pd) (μmol)	Pd equivalents	S_{BET} ($m^2\,g^{-1}$)	T_{max} (°C)	X(NO$_x$)$_{max}$ (%)	X(NO$_x$)$_{ov}$ (%)	S(N_2)$_{ov}$ (%)
0.14Pd/W/ZrO_2	640	1	56	180	60	40	86
0.27Pd/W/ZrO_2	1280	2	61	155	53	36	95
0.41Pd/W/ZrO_2	1922	3	62	160	55	33	96
0.55Pd/W/ZrO_2	2560	4	62	150	62	34	97
0.68Pd/W/ZrO_2	3200	5	55	150	56	34	95
0.82Pd/W/ZrO_2	3840	6	57	150	43	30	94

[a] The molar load of Pd refers to a catalyst mass of 500 mg used for the H_2-deNO$_x$ studies.
[b] Reaction conditions: m_{cat} = 500 mg, c(NO$_x$) = 500 vppm, c(H_2) = 2000 vppm, c(O_2) = 6 vol.%, Ar balance, F = 500 ml min^{-1} (STP), S.V. = 80,000 h^{-1}, β = 2 K min^{-1}.
[c] The load of W relates to the bare ZrO_2 carrier.

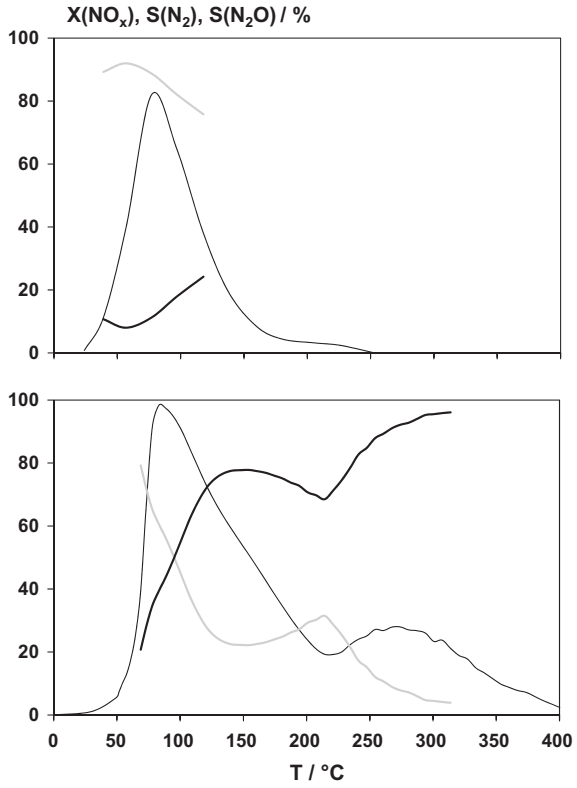

Fig. 1. H_2-deNO$_x$ performance of the reference catalysts 0.25Pt/Al_2O_3 (top) and 0.25Pt/W/ZrO_2 (bottom) (X(NO$_x$) —, S(N_2) —, S(N_2O) ——). Conditions: n_{Pt} = 640 μmol, m_{cat} = 500 mg, c(NO$_x$) = 500 vppm, c(H_2) = 2000 vppm, c(O_2) = 6 vol.%, Ar balance, F = 500 ml min^{-1} (STP), S.V. = 80,000 h^{-1}, β = 2 K min^{-1}.

4 W atoms nm^{-2} being in the range of monolayer surface coverage of approximately 4.5–5 W atoms nm^{-2} [30]. But, in HRTEM some disordered dots appear with a size of ca. 2 nm (Fig. 2, left). These flecks are also observed for the Pd-free W/ZrO_2 substrate, but not for bare ZrO_2. Although the resolution of the EDX detector was not sufficient to exactly assign these features to tungsten-enriched entities, it is likely that the nanoparticles correspond to distorted WO_3 entities. The coexistence of monolayer or sub-monolayer WO_x entities and distorted WO_3 nanoparticles has already been referred, whereas ordered crystalline WO_3 domains have only been reported for clearly higher loads of tungsten [30].

Like for tungsten EDX also indicates Pd all over the sample surface of 0.41Pd/W/ZrO_2 suggesting very small entities, whereas a clear identification of any Pd particles is not possible. We therefore estimate that the existing Pd or PdO_x particles are significantly smaller than 2 nm indicating a high dispersion on the substrate. Contrary, some Pd particles are clearly found on the 0.41Pd/Al_2O_3 reference catalyst showing a size of ca. 2 nm (Fig. 2, right). But, as for 0.41Pd/W/ZrO_2, EDX also displays Pd on the whole surface without clear localisation.

XPS investigations are conducted in order to obtain information on the chemical binding states. The binding energies measured for zirconia and tungsten oxide (Zr $3d_{5/2}$ = 183.0 eV, W $4f_{7/2}$ = 36.2 eV, O 1s = 531.0 eV) as well as for organic contaminants are in a good agreement with reference data and close to that reported in literature [31–33]. To prove the Pd load Fig. 3 exemplarily shows Pd $3d_{5/2}$ XP spectra of Pd/W/ZrO_2 catalysts with a Pd load of 0.41, 0.68 and 0.81%, which are superimposed by Zr $3p_{3/2}$ peaks. Nevertheless, both elements are clearly distinguishable. The main Pd $3d_{5/2}$ component at 337.4 eV is attributed to PdO, the weak component at 335.7 eV is assigned to Pd^0 and there is no evidence for Pd^+ formation [34]. Unfortunately, lower Pd contents are not amenable for XPS due to the insufficient detection limit. The major presence of PdO is in line with the thermodynamics, which

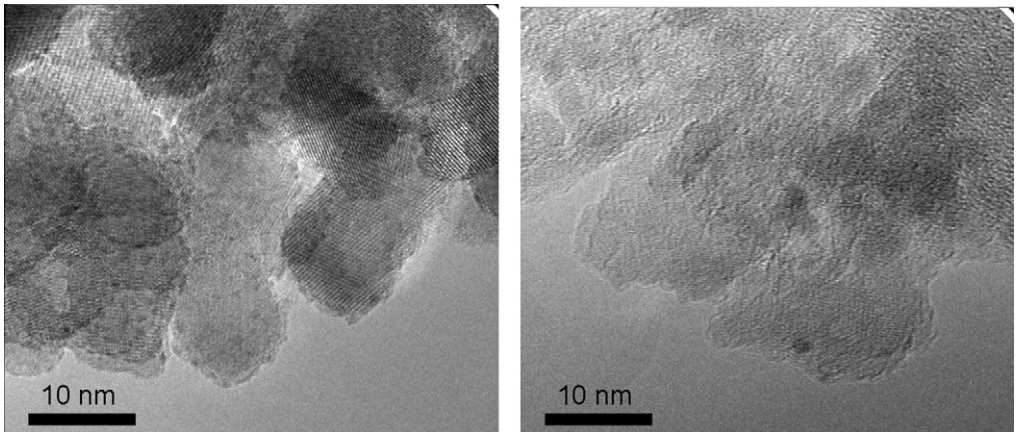

Fig. 2. Representative bright field HRTEM image of the catalyst 0.41Pd/W/ZrO_2 (left) and 0.14Pd/Al_2O_3 (right).

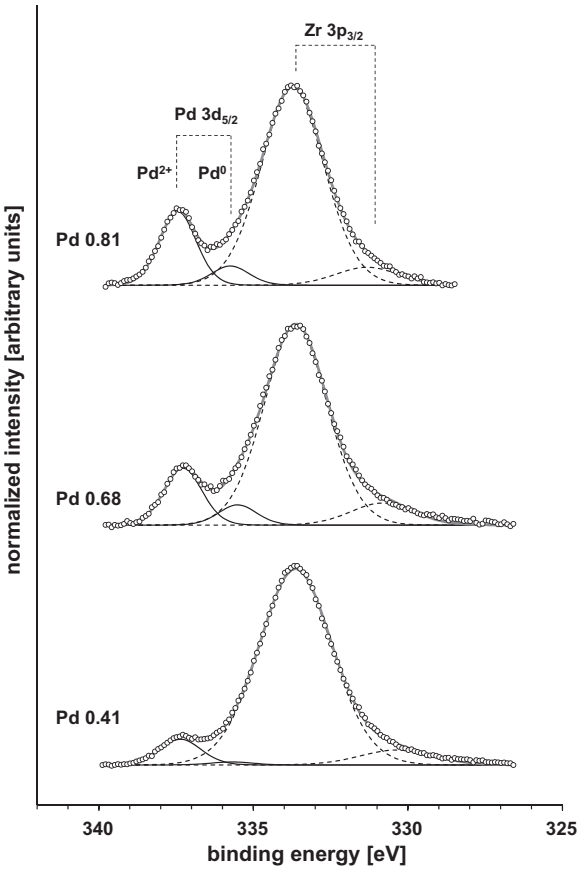

Fig. 3. XP spectra of the $Pd/W/ZrO_2$ catalysts with a Pd load of 0.41, 0.68 and 0.81%. Dots mark experimental points, whilst curves refer to the results of the multiplet fits (sum of sub-peaks ▬, Pd components —, Zr components - - -). For a better visualisation all spectra are normalised to maximum intensity.

evidences PdO to be the clearly favoured species under the conditions of preparation as well as catalytic studies as compared to elemental Pd. Equilibrium compositions were calculated with HSC Chemistry Software 5.1 from Outokumpu Research. The weak Zr $3p_{3/2}$ component at 331.0 eV is due to small amount of substoichiometric zirconia.

As expected, the BET surface area is very similar for all the $Pd/W/ZrO_2$ catalysts, as the present Pd contents are too low to affect the specific pore volume of the W/ZrO_2 substrate. However, the catalysts reveal a significantly decreased BET surface area as compared to bare ZrO_2 ($70\,m^2\,g^{-1}$). We have indicated in a previous paper [18] that this decline is mainly related to the mass of tungsten oxide, which contributes negligibly to the surface area only, and is not due to the blocking of pores of the ZrO_2 carrier.

The H_2-deNO_x studies show that all the $Pd/W/ZrO_2$ catalysts are active in a very similar temperature regime, i.e. $T_{x>20}$ approximately ranges from 125 to 285 °C. However, Table 1 indicates that the activity expressed as $X(NO_x)_{ov}$ tentatively decreases with growing Pd content. But, the efficiency at low temperatures rises when increasing the Pd load from 0.14 to 0.27% as displayed by the shifting of T_{max}, whereas with further increasing Pd proportion T_{max} remains very similar. Also, the maximum NO_x conversion does not significantly differ; an exception is the highest Pd loading (0.82%), which shows clearly diminished $X(NO_x)_{max}$. These results evidence that for pronounced low-temperature H_2-deNO_x activity a Pd load exceeding 0.14% is necessary, whereas Pd contents above 0.68% should be avoided due to suppression of H_2-deNO_x. We suppose that such high Pd loads imply larger PdO particles which rather support the competitive H_2–O_2 reaction.

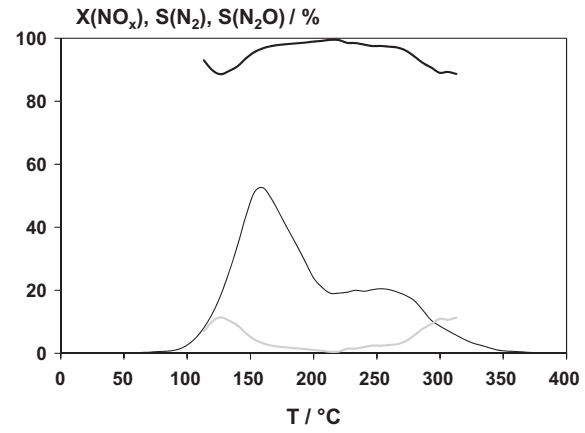

Fig. 4. H_2-deNO_x performance of the 0.41Pd/W/ZrO2 catalyst (X(NO_x) ▬, S(N2) - - -, S(N2O) ▬ ▬). Conditions: n_{Pd} = 1922 μmol (3 Pd equivalents), m_{cat} = 500 mg, $c(NO_x)$ = 500 vppm, c(H2) = 2000 vppm, c(O2) = 6 vol.%, Ar balance, F = 500 ml min^{-1} (STP), S.V. = 80,000 h^{-1}, β = 2 K min^{-1}.

Furthermore, a crucial result of the catalytic studies is the outstanding overall N_2 selectivity of the $Pd/W/ZrO_2$ samples, which ranges from 94 to 97% for Pd loads above 0.27%. For clarity, the H_2-deNO_x profile of $0.41Pd/W/ZrO_2$ is depicted in Fig. 4. This catalyst is considered to be a very promising sample combining remarkable performance in the low-temperature range with almost selective N_2 formation. At peak deNO_x the N_2 selectivity amounts to 96% corresponding to the production of 5 vppm N_2O only. Additionally, the $0.41Pd/W/ZrO_2$ catalyst was also evaluated under stationary conditions monitoring N_2 by GC/TCD (Fig. 5); note that in this test no NH_3 screened by FTIR was found. Table 2 compares the temperature-programmed and stationary experiments evidencing drastically higher H_2-deNO_x efficiency in steady-state. For example, at 160 °C $X(NO_x)_{max}$ is 90% under stationary conditions, whilst in the dynamic study it is 55%. Obviously, the heating rate of 2 K min^{-1} adjusted in the temperature-programmed runs is too fast to achieve steady-state on $0.41Pd/W/ZrO_2$. However, Table 2 shows that the experimental mode does not affect the N_2 selectivity. From the stationary data the apparent turnover frequency of the Pd sites is derived and compared with that of the highly active $0.25Pt/W/ZrO_2$ catalyst. As a result, the apparent TOF of $0.25Pt/11W/ZrO_2$ amounts to $1.2 \times 10^{-4}\,s^{-1}$ at 160 °C and a S.V. of 80,000 h^{-1} (specific rate of NO reduction: r_{NO} = 0.60 μmol $g_{Pt}^{-1}\,s^{-1}$), whilst for $0.41Pd/W/ZrO_2$ it is $8.1 \times 10^{-5}\,s^{-1}$ (r_{NO} = 0.76 μmol $g_{Pd}^{-1}\,s^{-1}$) thus indicating very

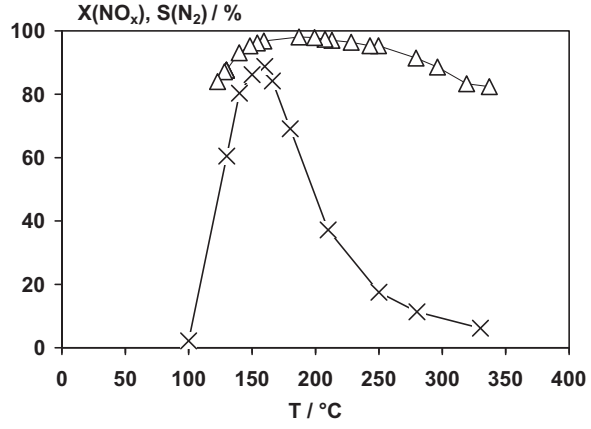

Fig. 5. Steady-state H_2-deNO_x performance of the $0.41Pd/W/ZrO_2$ catalyst (X(NO_x) ×, S(N_2) △). Conditions: n_{Pd} = 1922 μmol (3 Pd equivalents), m_{cat} = 500 mg, $c(NO_x)$ = 500 vppm, $c(H_2)$ = 2000 vppm, $c(O_2)$ = 6 vol.%, Ar balance, F = 500 ml min^{-1} (STP), S.V. = 80,000 h^{-1}.

Table 2
Comparison of the H_2-deNO$_x$ features of the 0.41Pd/W/ZrO_2 catalyst obtained from temperature-programmed and stationary[a,b].

	T_{max} (°C)	X(NO$_x$)$_{max}$ (%)	X(NO$_x$)$_{ov}$ (%)	S(N_2)$_{ov}$ (%)
Temperature-programmed	160	55	33	96
Stationary	160	90	60	94

[a] In temperature-programmed mode: $\beta = 2\,K\,min^{-1}$.
[b] Reaction conditions: $m_{cat} = 500$ mg, $c(NO_x) = 500$ vppm, $c(H_2) = 2000$ vppm, $c(O_2) = 6$ vol.%, Ar balance, $F = 500\,ml\,min^{-1}$ (STP), S.V. = 80,000 h^{-1}.

similar overall activity. However, at clearly lower temperatures the specific activity of Pt is much higher. For example at 100 °C, the 0.25Pt/W/ZrO_2 catalyst shows outstanding performance with a NO_x conversion of about 92% corresponding to an apparent TOF of $2.5 \times 10^{-4}\,s^{-1}$ ($r_{NO} = 1.3\,\mu mol\,g_{Pt}^{-1}\,s^{-1}$), whereas 0.41Pd/W/$ZrO_2$ reveals very minor performance only. Finally, it has to be mentioned that the Pt catalyst implies a clearly broader activity window; i.e. $T_{x>20}$ ranges from 65 to 325 °C, whilst for 0.41Pd/W/ZrO_2 it is from 125 to 280 °C.

The effect of H_2 on the NO_x reduction on 0.41Pd/W/ZrO_2 is investigated by varying the H_2 concentration from 1000 to 6000 vppm. Fig. 6 demonstrates mounting activity with growing H_2 content as indicated by increasing X(NO$_x$)$_{ov}$, X(NO$_x$)$_{max}$, range of $T_{x>20}$ as well as decreasing T_{max}. However, the overall selectivity of N_2 decreases markedly at high H_2 concentrations. In contrast to that, S(N_2)$_{ov}$ is not significantly affected when the content of O_2 varies from 3 to 18 vol.%. The H_2-deNO$_x$ performance remains the same for 3 and 6 vol.% O_2, but with further increasing O_2 it decreases drastically in terms of X(NO$_x$)$_{max}$, X(NO$_x$)$_{ov}$ and range of $T_{x>20}$ (Fig. 7). For example at 18 vol.% O_2, the conversion no more exceeds 20%. We interpret these results with the enhancement of the competitive H_2–O_2 reaction on Pd at high O_2 proportions thus suppressing the NO_x reduction. However, it should be mentioned that the temperature at maximum NO_x conversion is shifted to lower temperatures. We speculate that at low gas inlet temperatures the higher O_2 content, which accelerates the H_2 oxidation, leads to an increase in the local temperature of the catalyst bed supporting the H_2-NO_x reaction.

When a fraction of 10 vol.% H_2O is added to the standard feed, the H_2-deNO$_x$ efficiency of 0.41Pd/W/ZrO_2 investigated in steady-state is inhibited at low temperatures, i.e. the light-off is shifted to higher temperature as indicated by T_{max} (shift from 150 to 170 °C) and the range of $T_{x>20}$ (shift from ca. 110–240 °C to ca. 140–240 °C). However, X(NO$_x$)$_{max}$ as well as S(N_2) do not change significantly;

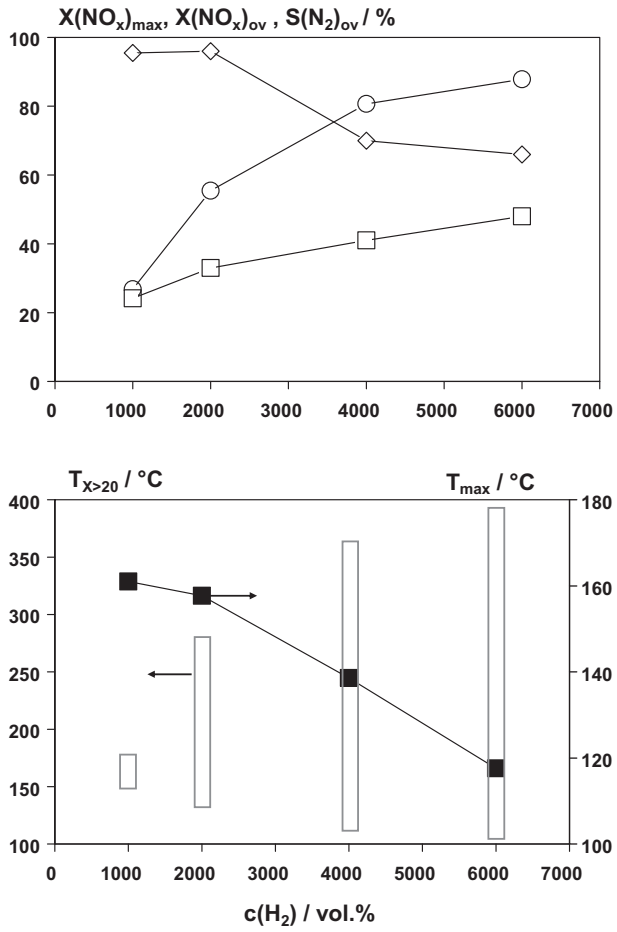

Fig. 6. Effect of H_2 on the H_2-deNO$_x$ performance of the 0.41Pd/W/ZrO_2 catalyst (X(NO$_x$)$_{max}$ (○), X(NO$_x$)$_{ov}$ (□), S(N_2)$_{ov}$ (◊), T_{max} (■), $T_{x>20}$ (□). Conditions: $n_{Pd} = 1922\,\mu mol$ (3 Pd equivalents), $m_{cat} = 500$ mg, $c(NO_x) = 500$ vppm, $c(H_2) = 2000.6000$ vppm, $c(O_2) = 6$ vol.%, Ar balance, $F = 500\,ml\,min^{-1}$ (STP), S.V. = 80′000 h^{-1}, $\beta = 2\,K\,min^{-1}$.

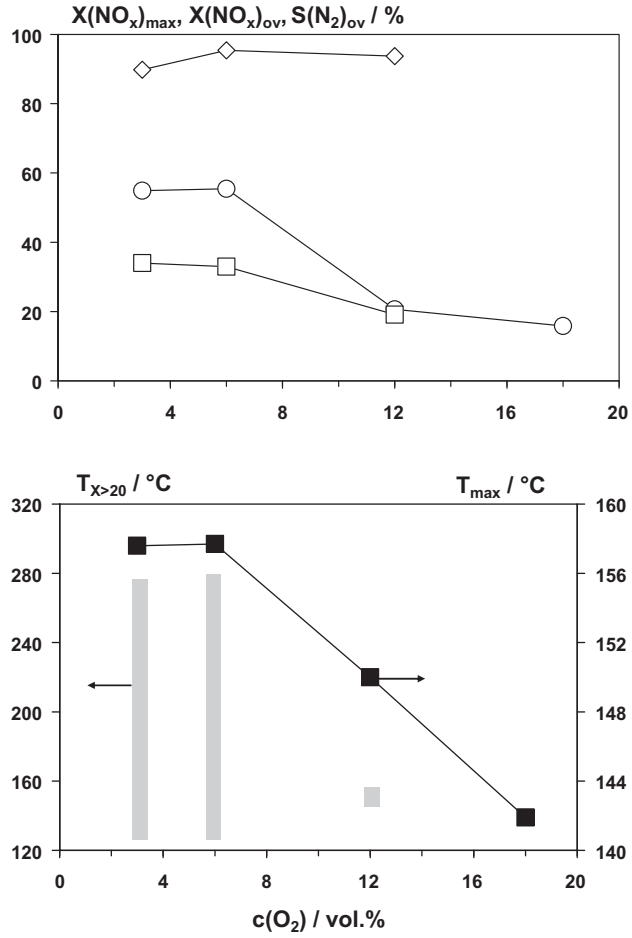

Fig. 7. Effect of O_2 on the H_2-deNO$_x$ performance of the 0.41Pd/W/ZrO_2 catalyst X(NO$_x$)$_{max}$ (○), X(NO$_x$)$_{ov}$ (□), S(N_2)$_{ov}$ (◊), T_{max} (■), $T_{x>20}$ (■). Conditions: $n_{Pd} = 1922\,\mu mol$ (3 Pd equivalents), $m_{cat} = 500$ mg, $c(NO_x) = 500$ vppm, $c(H_2) = 2000$ vppm, $c(O_2) = 3.18$ vol.%, Ar balance, $F = 500\,ml\,min^{-1}$ (STP), S.V. = 80,000 h^{-1}, $\beta = 2\,K\,min^{-1}$.

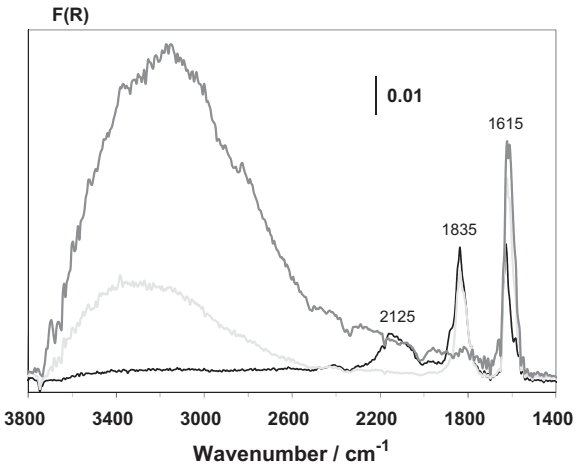

Fig. 8. DRIFT spectra of 0.41Pd/W/ZrO_2 recorded at 160 °C after exposure to 500 vppm NO_x and 6 vol.% O_2 and subsequent purging with N_2 (—) followed by supplying 500 vppm H_2 and 6 vol.% O_2 for 4 min ( ) and 12 min ( ).

also under wet conditions no evolution of NH_3 appeared as shown by FTIR. We assume that the inhibition below 140 °C is associated with the strong adsorption of H_2O on active sites of the catalyst.

The hydrothermal aging of the 0.41Pd/W/ZrO_2 catalyst performed for 24 h at 750 °C leads to clear decrease in the stationary H_2-deNO_x performance investigated in the standard feed gas; $X(NO_x)_{max}$ decreases from 90% (T_{max} at 160 °C) to 55% (T_{max} at 185 °C) and the range of $T_{x>20}$ is reduced and shifted from 125 to 280 °C to 130 to 220 °C. Also, the N_2 selectivity markedly decreases; $S(N_2)$ does not exceed 90% and $S(N_2)_{ov}$ diminishes from 94 to 80%. In contrast to 0.41Pd/W/ZrO_2, the related 0.3Pt/W/ZrO_2 sample shows no susceptibility towards hydrothermal treatment under very similar aging conditions [18]. It is therefore concluded that the hydrothermal aging exclusively refers to the deactivation of the catalytic active Pd sites.

3.2. Mechanism of the lean H_2-deNO_x reaction on 0.41Pd/W/ZrO_2

Mechanistic studies were performed with the 0.41Pd/W/ZrO_2 catalyst using DRIFT spectroscopy. In DRIFTS, the H_2-deNO_x reaction was temporally separated as described in Section 2.3. After the pre-treatment in N_2, the catalyst was exposed at 160 °C to the NO_x/O_2 mixture and was then flushed by N_2 resulting in a rather weak DRIFTS band between 2000 and 2225 cm^{-1} with a broad maximum at about 2125 cm^{-1}. This feature is attributed to NO^+, NO_2^+, $(NO)^{\delta+}$ or $(NO_2)^{\delta+}$ species coordinated to W^{6+} sites [18,35] (Fig. 8). The 2125 cm^{-1} band vanishes upon additional flushing for a couple of minutes indicating thermal desorption. Furthermore, intense DRIFTS features appear at 1635 and 1835 cm^{-1}. The former band refers to nitrite or nitrate species adsorbed on the W/ZrO_2 substrate [18], whilst the latter is ascribed to ν(NO) vibrations of NO linearly bonded to Pd^{2+} sites. Contrary, NO surface complexes, in which NO coordinates linearly or bent to Pd^+ or Pd^0 sites or bridges two or three sites, would appear significantly below 1800 cm^{-1} [36,37]. Obviously, the proportion of Pd^0 species indicated by XPS is too small to provide a significant NO vibration band. Preliminary studies performed with the bare W/ZrO_2 support show no DRIFTS feature between 1630 and 2000 cm^{-1}. This substantiates the assignment of the 1835 cm^{-1} band to NO chemisorbed on Pd sites. No band appears at 1925 cm^{-1}, which might be referred to N_2O_3 originated from NO oxidation on W^{6+} sites as reported recently [38].

When supplying the H_2/O_2 mixture, the signal at 1835 cm^{-1} vanishes demonstrating the participation of the Pd-NO complexes in the H_2-deNO_x reaction (Fig. 8). Note that even extended flushing with N_2 does not lead to removal of these species, contrary to NO_x adsorbed on tungsten oxide (2125 cm^{-1}) as shown in Fig. 8 as well. Additionally, the conversion of H_2 evidently results in the formation and adsorption of H_2O on the catalyst displayed by the growth of the broad band between 2400 and 3730 cm^{-1} (ν(OH)) and that of the feature at about 1615 cm^{-1} ($\delta(H_2O)$); we reported that the re-adsorption of H_2O mainly occurs on tungsten oxide [18]. Obviously, the band of the $\delta(H_2O)$ vibrations overlaps with the peak of the nitrite or nitrate species located on the substrate. We have lately shown by quantitative estimation of the DRIFTS bands that these species are not essentially involved in the lean H_2-deNO_x reaction on Pt/W/ZrO_2 [18]. However, due to the coincidence of the DRIFTS feature (1615 cm^{-1}) of adsorbed H_2O and surface nitrite/nitrate species the reaction of the latter cannot be excluded. Furthermore, it should be noticed that the DRIFTS investigations performed upon supply of the standard feed provide very similar vibration bands as referred to the sequential studies.

The DRIFT spectroscopic results prove the contribution of the Pd component in the H_2-deNO_x conversion under oxygen-rich conditions. We therefore suppose that this pathway follows the mechanism according to Burch including the reduction of active Pd sites by H_2 followed by adsorption and dissociation of NO. N_2 is subsequently produced by recombination of two N atoms, whereupon the oxygen is retained on the Pd sites [39]. Recently, we have suggested a very similar mechanism for lean H_2-deNO_x on Pt/W/ZrO_2 [18]. Nevertheless, as indicated in previous paragraph, some contribution of nitrite and nitrate species, respectively, located in close proximity to the Pd sites cannot be completely ruled out by the DRIFTS studies performed. Such a mechanism was postulated for H_2-deNO_x on Pt catalysts implying spill-over of hydrogen from active precious metal sites to neighbouring NO_x species chemisorbed on the substrate [15,16].

4. Conclusions

In this work, we presented a Pd/W/ZrO_2 catalyst for the lean H_2-deNO_x reaction being relevant for the NO_x abatement at low exhaust temperatures. The optimum Pd load was found to be 0.41%, whereas the content of W was 8.7%. This sample showed high activity between 125 and 250 °C implying an outstanding N_2 selectivity. It was also demonstrated that the catalyst showed higher performance under steady-state conditions. In conclusion, the 0.41Pd/W/ZrO_2 catalyst combines the high potential of the active component Pd and the W/ZrO_2 substrate both reported in literature for different H_2-deNO_x catalysts. However, as the efficiency of 0.41Pd/W/ZrO_2 was limited to a rather small operation window under the conditions adjusted (120–180 °C), its use in mobile applications, e.g. diesel engines, which require much broader range of activity, is difficult. Nevertheless, the catalyst is considered to be suitable for stationary applications such as power plants and industrial applications like nitric acid production.

Moreover, we studied the effect of H_2, O_2 and H_2O on the catalytic activity of 0.41Pd/W/ZrO_2. As a result, the optimum conditions in terms of high deNO_x and maximum N_2 selectivity included reduced O_2 content (≤6 vol.%) and rather low H_2 concentration (≤2000 vppm), whilst H_2O decreased the performance. Furthermore, the 0.41Pd/W/ZrO_2 catalyst revealed clear decrease in activity upon drastic hydrothermal exposure (24 h at 750 °C).

The physical–chemical characterisation of 0.41Pd/W/ZrO_2 showed that palladium predominately exists in the form of PdO, whilst tungsten is present in sub-monolayer WO_x entities as well as amorphous WO_3 nanoparticles both deposited on the tetragonal ZrO_2 carrier.

The mechanistic studies demonstrated that the lean H_2-deNO_x reaction occurs on the Pd sites. This includes dissociation of NO on Pd sites followed by release of N_2, whilst the formed oxygen remains on the Pd surface. Finally, the oxidised Pd sites are regenerated by H_2. Additionally, some participation of NO_x surface species chemisorbed in close proximity to the Pd sites cannot be excluded completely.

References

[1] M.V. Twigg, Appl. Catal. B 70 (2007) 2.
[2] R.M. Heck, R.J. Farrauto, S.T. Gulati, Catalytic Air Pollution, J. Wiley, New York, 2002.
[3] M. Köbel, M. Elsener, G. Madia, Ind. Eng. Chem. Res. 40 (2001) 52.
[4] Y. Huang, Y., Cheng, C. Lambert, SAE Technical Paper Series 2008-01-1021.
[5] P. Balle, B. Geiger, D. Klukowski, M. Pignatelli, S. Wohnrau, M. Menzel, I. Zirkwa, G. Brunklaus, S. Kureti, Appl. Catal. B 91 (2009) 587.
[6] D. Chatterjee, T., Burkhardt, M., Weibel, E., Tronconi, I., Nova, C. Ciardelli, SAE Technical Paper Series 2006-01-0468.
[7] N. Fekete, R., Kemmler, D. Voigtländer, B., Krutzsch, E., Room, G., Wenninger, W., Strehlau, J.A.A. van den Tillaart, J., Leyrer, E.S., Lox, W. Müller, SAE Paper 960133.
[8] F. Rohr, S.D. Peter, E. Lox, M. Kögel, A. Sassi, L. Juste, C. Rigaudeau, G. Belot, P. Gelin, M. Primet, Appl. Catal. B 56 (2005) 201.
[9] J.H. Jones, J.T. Kummer, K. Otto, M. Shelef, E.E. Weaver, Environ. Sci. Technol. 9 (1971) 791.
[10] E. Frank, H. Oguz, W. Weisweiler, Chem. Eng. Technol. 6 (2003) 679.
[11] K. Yokota, M. Fukui, T. Tanaka, Appl. Surf. Sci. 121/122 (1997) 273.
[12] N. Macleod, R.M. Lambert, Appl. Catal. B 35 (2002) 269.
[13] N. Macleod, R.M. Lambert, Appl. Catal. B 46 (2003) 483.
[14] C.N. Costa, V.N. Stathopoulos, V.C. Belessi, A.M. Efstathiou, J. Catal. 197 (2001) 350.
[15] C.N. Costa, P.G. Savva, C. Andronikou, P.S. Lambrou, K. Polychronopoulou, V.C. Belessi, V.N. Stathopoulos, P.J. Pomonis, A.M. Efstathiou, J. Catal. 209 (2002) 456.
[16] C.N. Costa, A.M. Efstathiou, J. Phys. Chem. C 111 (2007) 3010.
[17] C.N. Costas, P.G. Savva, J.L. Fierro, A.M. Efstathiou, Appl. Catal. B 75 (2007) 147.
[18] F.J.P. Schott, P. Balle, J. Adler, S. Kureti, Appl. Catal. B 87 (2009) 18.
[19] A. Tomita, T. Yoshii, S. Teranishi, M. Nagao, T. Hibino, J. Catal. 247 (2007) 137.
[20] A. Ueda, T. Nakao, M. Azuma, T. Kobayashi, Catal. Today 45 (1998) 135.
[21] G. Qi, R. Yang, L. Thompson, Appl. Catal. A 259 (2004) 261.
[22] G.L. Chiarello, D. Ferri, J.-D. Grunwaldt, L. Forni, A. Baiker, J. Catal. 252 (2007) 137.
[23] G.L. Chiarello, J.-D. Grunwaldt, D. Ferri, R. Krumeich, C. Oliva, L. Forni, A. Baiker, J. Catal. 252 (2007) 127.
[24] T. Nakatsuji, J. Ruotoistenmäki, M. Matsubara, T. Uekusa, Y. Tanaka, SAE Technical Paper Series 2003-01-3243.
[25] K.L. Parry, A.G. Shard, R.D. Short, R.G. White, J.D. Whittle, A. Wright, Surf. Interface Anal. 38 (2006) 1497.
[26] J.H. Scofield, J. Electron Spectrosc. Relat. Phenom. 8 (1976) 129.
[27] S. Tanuma, C.J. Powell, D.R. Penn, Surf. Interface Anal. 21 (1994) 165.
[28] C.N. Satterfield, Mass Transfer in Heterogeneous Catalysis, Colonial Press Clinton, 1977.
[29] D.E. Mears, Ind. Eng. Chem. Process Res. Dev. 10 (1971) 541.
[30] E.I. Ross-Medgaarden, W.V. Knowles, T. Kim, M.S. Wong, W. Zhou, C.J. Kiely, I.E. Wachs, J. Catal. 256 (2008) 108.
[31] B.M. Reddy, G.K. Reddy, K.N. Rao, L. Katta, J. Mol. Catal. A: Chem. 306 (2009) 62.
[32] T. Nishigushi, K. Oka, T. Matsumoto, H. Kanai, K. Utani, S. Imamura, Appl. Catal. A 301 (2006) 66.
[33] J.F. Moulder, W.F. Stickle, P.E. Sobol, K.D. Bomben, Handbook of X-Ray Photoelectron Spectroscopy, 2nd ed., Perkin Elmer Corp., Eden Prairie, MN, 1992.
[34] G.B. Hoflund, H.A.E. Hagelin, J.F. Weaver, G.N. Salaita, Appl. Surf. Sci. 205 (2003) 102.
[35] A.A. Davydov, Infrared Spectroscopy of Adsorbed Species on the Surface of Transition Metal Oxides, John Wiley, New York, 1990.
[36] M. Valden, R. Keiski, N. Xiang, J. Pere, J. Aaltonen, M. Pessa, T. Maunula, A. Savimäki, A. Lathi, M. Härkönen, J. Catal. 161 (1996) 614.
[37] T.E. Hoost, K. Otto, K.A. Laframboise, J. Catal. 155 (1995) 303.
[38] M. Kantcheva, I. Cayirtepe, J. Mol. Catal. A 247 (2006) 88.
[39] R. Burch, P.J. Millington, A.P. Walker, Appl. Catal. B 4 (1994) 65.